

Dissecting the Main Sequence: AGN Activity and Bulge Growth in the Local Universe

C. McPartland¹★, D. B. Sanders¹, L. J. Kewley², S. K. Leslie³

¹*Institute for Astronomy, 2680 Woodlawn Dr., Honolulu, HI 96822, USA*

²*Research School of Astronomy & Astrophysics, Australian National University, Cotter Road, Weston, ACT 2611, Australia*

³*Max-Planck Institut für Astronomie, Königstuhl 17, D-69117, Heidelberg, Germany*

Accepted 2018 October 19. Received 2018 October 3; in original form 2018 June 30

ABSTRACT

Local galaxies from the Sloan Digital Sky Survey are used to provide additional support for an evolutionary pathway in which AGN activity is associated with star-formation quenching. Composite, Seyfert 2 and LINER galaxies account for ~60% of all star-formation in massive galaxies ($M_{\star} > 10^{10.5} M_{\odot}$). Inclusion of these galaxies results in a “turnover” in the $SFR-M_{\star}$ relation for massive galaxies. Our analysis shows that bulge growth has already occurred in the most massive galaxies ($M_{\star} > 10^{10.5} M_{\odot}$), and bulges continue to grow as galaxies quench and redden, $(g-r) = 0.5 \rightarrow 0.75$. Significant bulge growth is also occurring in low mass starburst galaxies ($M_{\star} < 10^{10.5} M_{\odot}$) at 0.5 dex above the “main sequence” (MS), where we find an increase in B/T from 0.1 \rightarrow 0.3 and bluer colours, $(g-r) < 0.25$ compared to low-mass galaxies on the MS.

Key words: galaxies:evolution — galaxies:star-formation — galaxies:active — galaxies:bulges — galaxies:structure — galaxies:Seyfert

1 INTRODUCTION

Over the past decade, it has become clear that the star-formation rates (SFR) and stellar masses (M_{\star}) of star-forming galaxies are highly correlated. Early studies revealed the existence of a roughly linear $SFR-M_{\star}$ relation for star-forming galaxies to at least $z \sim 2$; and gave the relation the name the star-forming galaxy “main sequence” (hereafter the MS; Noeske et al. 2007; Daddi et al. 2007; Elbaz et al. 2007). The salient features of the MS from these early studies are that normalization of the MS increases with redshift, while the intrinsic scatter in the relation appeared to be small (0.2 - 0.3 dex) at all redshifts studied (Speagle et al. 2014). It was argued that the existence of the MS implied that star-formation was regulated by a limited set of internal processes, (e.g. gas supply), followed by an additional unknown process that “quenches” the galaxy (e.g. gas exhaustion); transforming the galaxy in colour from blue to red.

Oemler et al. (2017) demonstrate that most star-formation history models will produce a tight main sequence, and thus yield little astrophysical insight. However, the properties of the quiescent population require additional astrophysical processes to explain. Early studies, which generally excluded AGN from their analysis, argued that bulge size and local environmental density were the best predictors of

quenching (e.g. Cheung et al. 2012; Fang et al. 2013; Omand et al. 2014). With the availability of data from the Spitzer and Herschel space telescopes, studies using large samples of robust mid- and far-IR based SFR measurements uncovered a flattening, or “turnover”, in the slope of the MS above $M_{\star} \approx 3 \times 10^{10} M_{\odot}$ in local galaxies (Salim et al. 2007) as well as at higher redshifts (Whitaker et al. 2014; Lee et al. 2015; Tomczak et al. 2016).

The existence of a turnover in the MS implies that massive galaxies have lower average SFRs than would be expected if there were a linear MS. Abramson et al. (2014) argue that the “turnover” in the MS may be a result of the increased bulge mass-fractions in massive galaxies, which causes the total M_{\star} to be a poor proxy for the star-forming gas, which primarily resides in the disk. More recently, Leslie et al. (2016, hereafter L16) have reanalyzed the SFR data for SDSS galaxies by galaxy spectral type, and have shown that Composites, Seyfert 2, and LINER galaxies form a “quenching pathway” for massive galaxies, which is nearly perpendicular to the star-forming MS, suggesting that active galactic nuclei (AGN) may play a key role in quenching star formation and removing massive galaxies from the MS.

In this *letter*, we continue to use SDSS data to further explore the nature of the “turnover” in the MS due both to AGN and bulge growth in massive galaxies. Specifically, we use the subset of the L16 sample with bulge+disk photometry from Simard et al. (2011, hereafter S11) to address two main questions: 1) Which galaxies produce the turn over in

★ E-mail: conormcp@ifa.hawaii.edu (CM)

the MS at high M_\star ? Is the “turnover” a result of sample biases, or an indication of a different mechanism regulating star-formation in massive galaxies?, and 2) What makes a disk galaxy grow a bulge, and how is the growth of that bulge related to AGN activity and quenching? The data sample and spectral classification methods are reviewed in §2. The results are presented in §3, and discussed in §4. A summary of our analysis and conclusions are given in §5.

2 DATA SAMPLE

Our galaxy sample is drawn from the SDSS data release 7 (Abazajian et al. 2009). Redshifts from the S11 bulge+disk decomposition catalogue are used to select galaxies between redshifts $z = 0.04$ and 0.1 (as in L16). For each of the selected galaxies, we extract the r -band bulge-to-total fraction, B/T and total gr absolute magnitudes, $M_{g,g}$, $M_{r,g}$. We use the “n4”-model from S11 which assumes a de Vaucouleurs/exponential profile for the bulge/disk, and is more robust than the “fn”-model which uses a Sèrsic profile for the bulge. We considered using stellar mass B/T ratios from the catalog of Mendel et al. (2014), but found that the average errors on these measurements are too large for the analysis presented in this letter.

Star-formation rates, stellar masses, and emission line fluxes are extracted from the MPA/JHU SDSS DR7 catalogues¹. Star-formation rates in the MPA/JHU catalogue are measured using the method (Brinchmann et al. 2004) which relies on dust-corrected $H\alpha$ luminosities for star-forming galaxies, and an empirical relation between D4000 and specific SFR (SFR/M_\star) for the remaining sources. Stellar masses estimates are based on fits to the photometry following Kauffmann et al. (2003). Here, we use the catalogue version 5.2b, but note little difference from the original measurements. Aperture corrections in the MPA/JHU catalogues are applied to SFR s and stellar mass estimates following Salim et al. (2007). We adopt the median estimates for SFR and M_\star . The entire analysis was repeated using SFR estimates from Ellison et al. (2016), as well as SFR and M_\star estimates from the Galex-SDSS-WISE Legacy Catalogue (GSWLC: Salim et al. 2016). Here, we adopt the MPA/JHU measurements since they provide the largest galaxy sample, and a direct comparison with studies already in the literature.

There are 290,976 sources at $z = 0.04$ – 0.1 with measurements of $[M_\star, SFR]$ from the MPA/JHU catalogue, and $[B/T, M_{g,g}, M_{r,g}]$ from the S11 catalogue. Since spectral classification is essential to our analysis, following L16, passive galaxies (i.e. sources with $H\alpha$ S/N < 3) are removed from the BPT analysis. This results in a final sample of 203,162 galaxies in the desired redshift interval with satisfactory measurements of SFR , M_\star , B/T , $(g-r)$ colour, and emission line ratios.

2.1 Spectral Classification

Following L16, we adopt the Kewley et al. (2006) classification scheme, which builds on diagnostic diagrams proposed by Baldwin et al. (1981); Veilleux & Osterbrock (1987) to

classify to the dominant source of ionizing flux in an emission line galaxy. We use the emission line ratios $[N\text{ II}]/H\alpha$, $[S\text{ II}]/H\alpha$, $[O\text{ I}]/H\alpha$, and $[O\text{ III}]/H\beta$ to divide our sample into four spectral classes: Star-Forming, Composite, Seyfert 2, and LINER galaxies. We exclude ambiguous galaxies – i.e. those with conflicting classifications – from the BPT analysis (e.g. Composite in $[O\text{ III}]/H\beta$ – $[N\text{ II}]/H\alpha$ but Seyfert 2 in $[O\text{ III}]/H\beta$ – $[S\text{ II}]/H\alpha$). The ambiguous galaxies are included in Fig. 2 to simply provide an accurate measure of the passive galaxy fraction.

3 THE SFR – M_\star DIAGRAM BY SPECTRAL CLASS

In this section, we present the distribution of each spectral class in the SFR – M_\star diagram. For each spectral class, we divide galaxies into 0.1×0.1 dex bins of $\Delta \log SFR \times \Delta \log M_\star$. In Fig. 1, the colour scale indicates the logarithm of the number of galaxies in each bin. The panels from left to right show Star-Forming, Composite, Seyfert 2, and LINER galaxies. The numbers in each panel indicate the total number of galaxies in our sample with the corresponding spectral classification. The dashed contours show the 25,50,90,99% quantiles of the Gaussian smoothed joint distribution in SFR – M_\star for the respective spectral class.

The SFR – M_\star relation for Star-Forming galaxies provides a useful benchmark to understand how other spectral classes differ. The solid black lines in each panel of Fig. 1 indicate the median and 10,90% quantiles in SFR as a function of M_\star for Star-Forming galaxies (see § 3.1, same as the blue line in Fig. 2); the white lines show the same for Composite, Seyfert 2, and LINER galaxies. The red line indicates the median SFR for passive galaxies in our sample (see § 2). The median SFR for Composite galaxies with stellar masses $\gtrsim 10^{10.5} M_\odot$ is a factor of ~ 2 lower than Star-Forming galaxies in the same mass interval. However, the Composite galaxy distribution has broad tails that extend up to the highest SFR s in our sample, and down to SFR s consistent with the quenched population. Seyfert 2 galaxies above $10^{10.5} M_\odot$ have a median SFR an additional factor ~ 3 lower than Composite galaxies, but have a similar median stellar mass of $M_\star \sim 6 \times 10^{10} M_\odot$. LINER galaxies have a slightly larger median stellar mass around $M_\star \sim 7.5 \times 10^{10} M_\odot$, with an additional factor of ~ 3 decrease in SFR compared to Seyfert 2 galaxies.

3.1 The turnover in SFR – M_\star at high M_\star

We split galaxies into bins of $\Delta \log M_\star$, and show the fraction of galaxies from each spectral type in the top panel of Fig. 2. For completeness, we include passive and ambiguous galaxies (see § 2 & 2.1). Star-Forming galaxies represent the majority of the galaxy population at lower stellar masses, but galaxies classified as Composite, Seyfert 2, and LINER outnumber them above a stellar mass of $M_\star \sim 10^{10.6} M_\odot$. We next investigate how including these “non-Star-Forming” galaxies influences measurements of the MS.

To determine the shape of the MS, we compute the median SFR as a function of M_\star using natural width bins of 2000 galaxies each. We begin with only Star-Forming galaxies and then repeat the calculation after adding Composite,

¹ <http://www.mpa-garching.mpg.de/SDSS/DR7/>

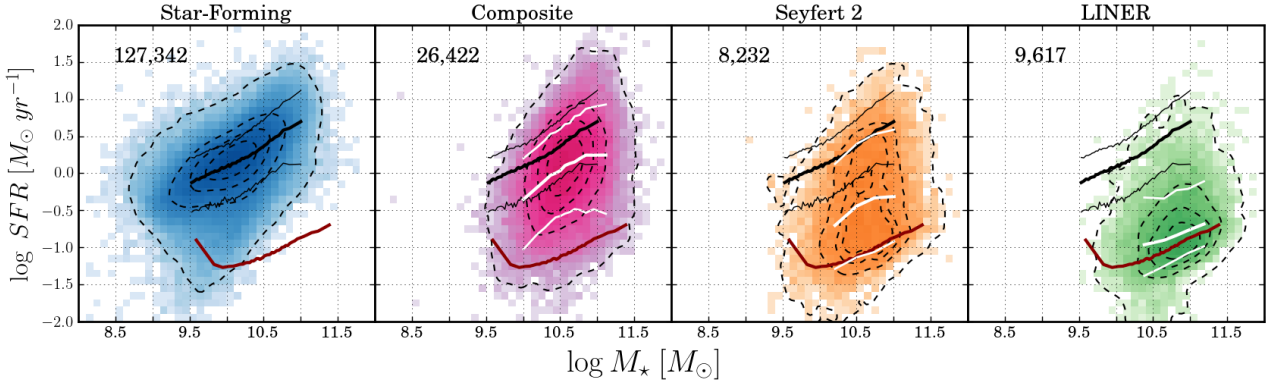


Figure 1. The logarithmic number density of galaxies by spectral class in 40×40 bins of $\Delta SFR \times \Delta M_*$. The top of each panel shows the name and sample size of the respective class. The dashed contours encompass 25, 50, 90, 99 percent of the sources in each panel. The solid black lines indicate the median and 10/90% quantiles in SFR as a function of M_* for Star-Forming galaxies. The white lines show the same for the other three classes. The red line indicates the median SFR for passive galaxies.

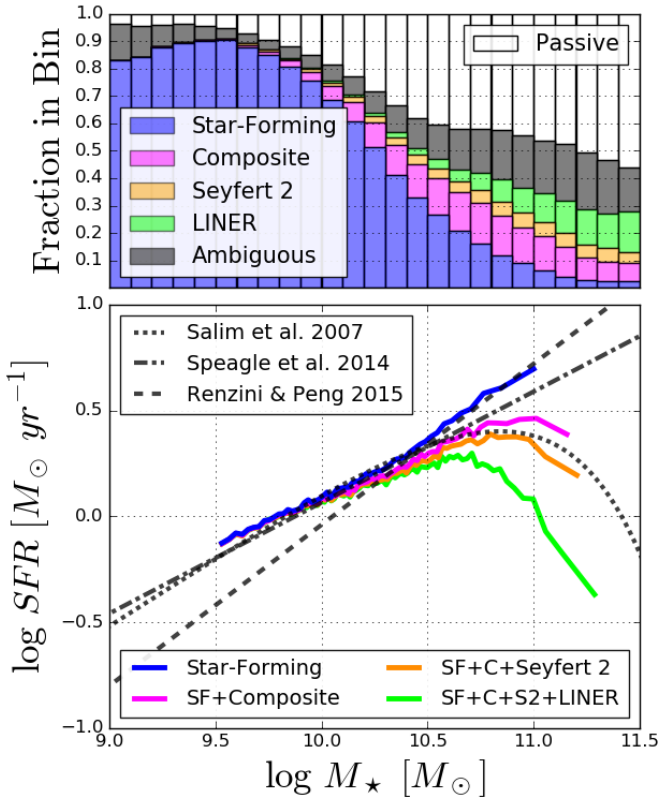


Figure 2. *top:* The fraction of galaxies classified as Star-Forming, Composite, Seyfert 2, LINER, ambiguous, and passive in bins of stellar mass. *bottom:* The median star-formation rate as a function of stellar mass for galaxies in four subsets of spectral classes (coloured lines). The dashed and dotted lines show measurements from the studies indicated at the top left.

Seyfert 2, and LINER galaxies. We show the results of this exercise in the bottom panel of Fig. 2. The MS considering only Star-Forming galaxies is roughly linear with slope and normalization consistent with Renzini & Peng (2015), as well as Elbaz et al. (2007, after converting back to a Kroupa

IMF). Adding Composite and Seyfert 2 galaxies flattens the MS at high stellar masses producing a relation consistent with the MS for all galaxies found by Salim et al. (2007), and similar to other results at higher redshifts (e.g. Whitaker et al. 2014; Lee et al. 2015; Tomczak et al. 2016).

The growth of a central bulge could also produce the high-mass turnover in the MS. Abramson et al. (2014) show the local MS straightens if one removes the mass of the bulge from the total mass. At higher redshifts, bulge dominated galaxies have also been shown to flatten the high mass end of the $SFR-M_*$ relation Whitaker et al. (2015); Erfanianfar et al. (2016). However, since supermassive blackholes and bulges maintain an approximately constant mass ratio, many authors argue that the anti-correlation between bulge-fraction and SFR supports a paradigm in which AGN feedback quenches star-formation (Bell et al. 2012; Bluck et al. 2014, 2016; Lang et al. 2014; Teimoorinia et al. 2016; Brennan et al. 2017). In the next section, we investigate how both bulge fraction and AGN activity relate to the SFR s of local galaxies.

4 BULGE/TOTAL AND GALAXY COLOUR IN THE $SFR-M_*$ DIAGRAM

We present the bulge/total fractions and galaxy colours of each spectral class in the $SFR-M_*$ diagram. We calculate the median B/T , and galaxy $(g-r)$ colours in each of the bins used in Fig. 1. The top and bottom panels of Fig. 3 show the result of this calculations for B/T and galaxy $(g-r)$ colour. The colour scale in the top panel indicates the median B/T with dark blue corresponding to a pure-disk galaxy with $B/T = 0$, and brown corresponding to a bulge-dominated galaxy with $B/T = 2/3$. The colour scale in the bottom panel of Fig. 3 indicates the median rest-frame $(g-r)$ colour for the galaxies in each bin. Following definitions from Mendel et al. (2014), who used a similar sample of SDSS galaxies, purple corresponds with $(g-r) = 0.1$, the colour of the bluest galaxies in the Blue Cloud; red corresponds with $(g-r) = 0.8$, the colour of the Red Sequence at $M_* \sim 10^{11} M_\odot$; and green corresponds with $(g-r) = 0.6$, the colour of the Green

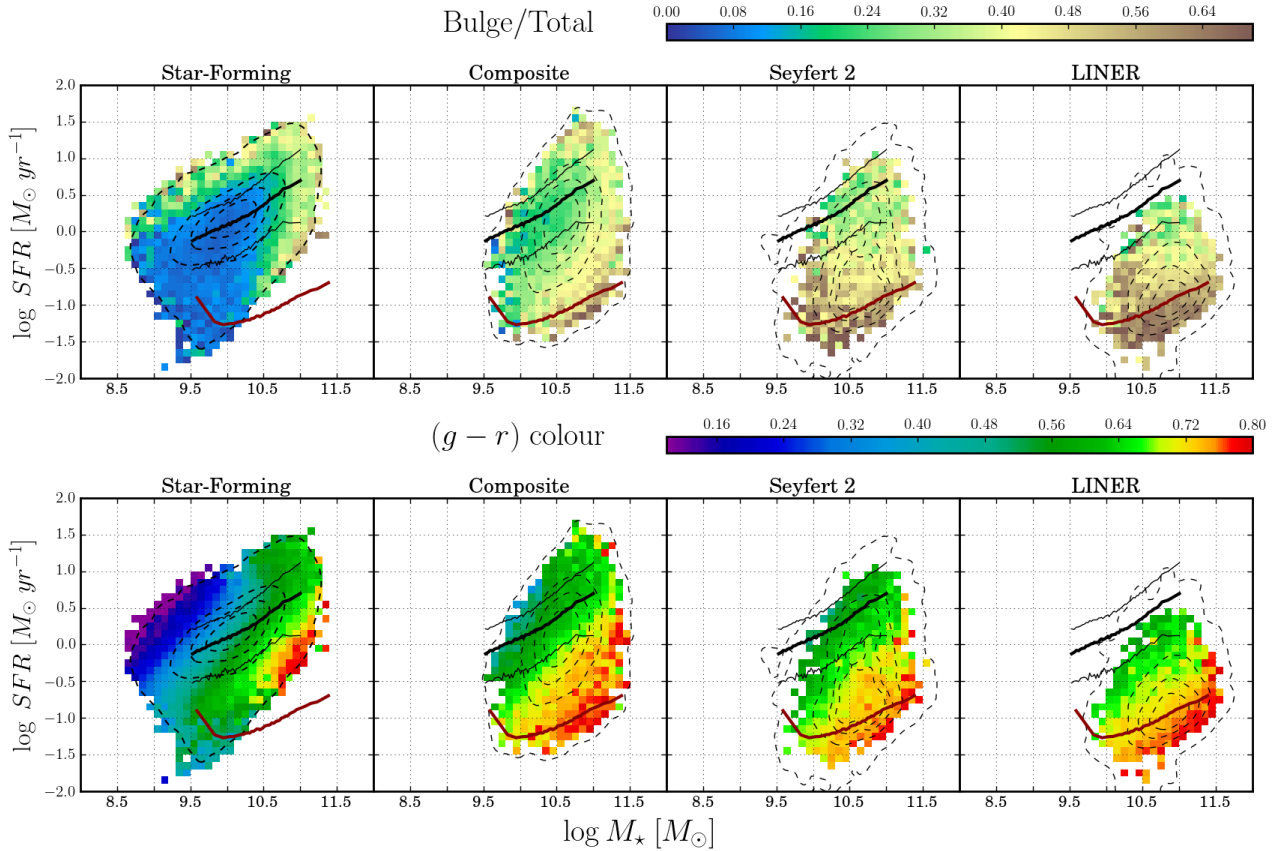


Figure 3. The median bulge-to-total fraction, B/T (top), and $(g-r)$ colour (bottom) using the same bins as in Fig. 1. Here, we reproduce the contours, and median/quantile lines from Fig. 1 (although we omit the white lines for clarity). Note that the B/T measurements for individual galaxies do indeed range from 0 to 1. However, we limit the B/T colour range to 0–2/3 to highlight the dynamic range of the medians.

Valley at $M_{\star} \sim 10^{10} M_{\odot}$. The dashed contours and solid lines (black and red) are the same as in Fig. 1.

There is a sharp $\sim 30\text{--}40\%$ increase in the median B/T for Star-Forming galaxies with star-formation rates $\gtrsim 3$ times higher than the median for their stellar mass. There is a similarly sharp increase in B/T at all SFR s above a stellar mass of $M_{\star} \sim 10^{10.5} M_{\odot}$. Wuyts et al. (2011) find similar trends in the Sérsic indices of local SDSS galaxies. The medians in B/T for the remaining spectral classes are $\gtrsim 30\%$ throughout most the SFR – M_{\star} diagram. Bulge fractions for Composite galaxies increase above the MS, but peak at the lowest SFR s and highest masses. The median B/T of Seyfert 2 and LINER galaxies increases with decreasing SFR , as well with decreasing stellar mass. This is the opposite trend than what we find for Star-Forming galaxies, and could possibly be due to emission from an AGN that has not been accounted for in the S11 bulge+disk decompositions. Deeper imaging data with a smaller PSF FWHM than SDSS will help to disentangle emission in the bulge from that of a compact nucleus.

The $(g-r)$ colours of Star-Forming galaxies with stellar mass $M_{\star} \lesssim 10^{10.5} M_{\odot}$ in general correlate inversely with specific star-formation rate (i.e. SFR/M_{\star}). The exception being low-mass low- SFR galaxies with $M_{\star} \sim 10^{9.5} M_{\odot}$ and $SFR \sim 0.03\text{--}0.1 M_{\odot}\text{yr}^{-1}$ where the median $(g-r)$ colours are similar to MS galaxies of the same mass. However, this may be an artefact of incompleteness in the SDSS spectroscopic

sample at these low masses and star-formation rates. More massive Star-Forming galaxies above the MS have green median colours of $(g-r) \sim 0.6$; consistent with “Green Valley” galaxies. The median colours of massive Star-Forming galaxies with the lowest SFR are consistent with the Red Sequence despite featuring Milky Way level star formation rates of $SFR \sim 1 M_{\odot}\text{yr}^{-1}$.

Composite and Seyfert 2 galaxies with SFR greater than the median for their mass and spectral type also feature median colours that would place them in the Green Valley. LINER galaxies in the top 10th percentile in SFR have similar colours as well. Red Composite galaxies have a broader distribution in SFR than either Seyfert 2 or LINER galaxies; suggesting Composite galaxies may have more dust, and thus more reddening, than other galaxies of similar SFR and M_{\star} . Seyfert 2 and LINER galaxies get redder as specific SFR decreases, with a weak trend toward bluer colours with decreasing stellar mass.

5 CONCLUSIONS

We use SDSS-DR7 galaxies with bulge+disk decomposition from S11 to investigate how the bulge/total (B/T) ratio of galaxies varies as a function of galaxy spectral type and location in the $SFR - M_{\star}$ diagram. We also show how the

inclusion of star-formation from galaxies of different spectral types affects the mean $SFR - M_\star$ relation at high M_\star . Our main findings are given below.

(i) For massive galaxies ($M_\star > 10^{10.5} M_\odot$), the fraction classified as either Composite, Seyfert 2 or LINER increases systematically with increasing M_\star , reaching $>50\%$ at $M_\star > 10^{10.5} M_\odot$; therefore, samples selected to contain only galaxies classified as “pure star-forming” miss a significant fraction of the massive galaxy population. Nearly 60% of the total star formation in galaxies with $M_\star \gtrsim 10^{10.5} M_\odot$ occurs in galaxies classified as non-star-forming (i.e. Composite, Seyfert 2, or LINER).

(ii) Galaxies classified as Composite cover a broad range in SFR, extending up to 1 dex above the MS (consistent with powerful starbursts), and up to 2 dex below the MS (consistent with passive galaxies). Including Composite galaxies when computing the median $SFR(M_\star)$ flattens the $SFR - M_\star$ relation above $M_\star = 10^{10.5} M_\odot$ and creates a negative slope (i.e. “turnover”) above $M_\star = 10^{11} M_\odot$. Further inclusion of Seyfert 2 and LINER galaxies pushes the the turnover point to lower M_\star .

(iii) For low-mass star-forming galaxies ($M_\star < 10^{10.5} M_\odot$), the median B/T increases sharply ($0.1 \rightarrow 0.3$) at $SFR \sim 0.5$ dex above the MS. These galaxies have bluer colours, $(g - r) < 0.25$, than their MS counterparts, $(g - r) \sim 0.3 - 0.5$.

(iv) All massive galaxies ($M_\star > 10^{10.5} M_\odot$) have median $B/T > 0.3$ and green to red colours, $(g - r) > 0.5$. Composite galaxies show a clear trend of increased B/T (> 0.4) above $M_\star \sim 10^{11}$. The largest bulges, $B/T > 0.5$, and the reddest colors, $(g - r) > 0.75$, are both found in galaxies with $SFR \gtrsim 1.5$ dex below the MS.

Our results further demonstrate that AGN activity is associated with star-formation quenching in massive galaxies, and strongly suggest that bulge growth is an integral part of this quenching pathway. Future work with deeper and higher resolution imaging data will be necessary to better address the possible connections between AGN and bulge growth in quenching star-formation. The Pan-STARRS 1 (PS1) 3π survey (Chambers et al. 2016) will allow better decomposition of galaxy radial profiles (Lokken et al. 2018). Large spatially resolved integral field spectroscopy data sets, such as those provided by MaNGA (Bundy et al. 2015) and SAMI (Croom et al. 2012) will also help to shed light on this issue by allowing studies of the spatial distribution of star-formation in relation to BPT classifications.

ACKNOWLEDGEMENTS

The authors would like to thank the anonymous referee for the very helpful comments that greatly improved the quality of the manuscript. Funding for the SDSS and SDSS-II has been provided by the Alfred P. Sloan Foundation, the Participating Institutions, the National Science Foundation, the U.S. Department of Energy, the National Aeronautics and Space Administration, the Japanese Monbukagakusho, the Max Planck Society, and the Higher Education Funding Council for England. The SDSS Web Site is <http://www.sdss.org/>. D.S. would like to thank the Distinguished Visitor Program at the Research School for As-

tronomy and Astrophysics, Australian National University for their generous support while in residence at the Mount Stromlo Observatory, Weston Creek, ACT. C.M. and D.S. also acknowledge support from NSF grant number 1716994. The work of D.S. was performed in part at the Aspen Center for Physics, which is supported by National Science Foundation grant PHY-1607611.

REFERENCES

- Abazajian K. N., et al., 2009, *ApJS*, **182**, 543
Abramson L. E., Kelson D. D., Dressler A., Poggianti B., Gladders M. D., Oemler J. A., Vulcani B., 2014, *ApJ*, **785**, L36
Baldwin J. A., Phillips M. M., Terlevich R., 1981, *PASP*, **93**, 5
Bell E. F., et al., 2012, *ApJ*, **753**, 167
Bluck A. F. L., Mendel J. T., Ellison S. L., Moreno J., Simard L., Patton D. R., Starkeburg E., 2014, *MNRAS*, **441**, 599
Bluck A. F. L., et al., 2016, *MNRAS*, **462**, 2559
Brennan R., et al., 2017, *MNRAS*, **465**, 619
Brinchmann J., Charlot S., White S. D. M., Tremonti C., Kauffmann G., Heckman T., Brinkmann J., 2004, *MNRAS*, **351**, 1151
Bundy K., et al., 2015, *ApJ*, **798**, 7
Chambers K. C., et al., 2016, preprint, ([arXiv:1612.05560](https://arxiv.org/abs/1612.05560))
Cheung E., et al., 2012, *ApJ*, **760**, 131
Croom S. M., et al., 2012, *MNRAS*, **421**, 872
Daddi E., et al., 2007, *ApJ*, **670**, 156
Elbaz D., et al., 2007, *A&A*, **468**, 33
Ellison S. L., Teimoorinia H., Rosario D. J., Mendel J. T., 2016, *MNRAS*, **455**, 370
Erfanianfar G., et al., 2016, *MNRAS*, **455**, 2839
Fang J. J., Faber S. M., Koo D. C., Dekel A., 2013, *ApJ*, **776**, 63
Kauffmann G., et al., 2003, *MNRAS*, **341**, 33
Kewley L. J., Groves B., Kauffmann G., Heckman T., 2006, *MNRAS*, **372**, 961
Lang P., et al., 2014, *ApJ*, **788**, 11
Lee N., et al., 2015, *ApJ*, **801**, 80
Leslie S. K., Kewley L. J., Sanders D. B., Lee N., 2016, *MNRAS*, **455**, L82
Lokken M. E., McPartland C., Sanders D. B., 2018, in American Astronomical Society Meeting Abstracts #231. p. #354.03
Mendel J. T., Simard L., Palmer M., Ellison S. L., Patton D. R., 2014, *ApJS*, **210**, 3
Noeske K. G., et al., 2007, *ApJ*, **660**, L43
Oemler Jr. A., Abramson L. E., Gladders M. D., Dressler A., Poggianti B. M., Vulcani B., 2017, *ApJ*, **844**, 45
Omand C. M. B., Balogh M. L., Poggianti B. M., 2014, *MNRAS*, **440**, 843
Renzini A., Peng Y.-j., 2015, *ApJ*, **801**, L29
Salim S., et al., 2007, *ApJS*, **173**, 267
Salim S., et al., 2016, *ApJS*, **227**, 2
Simard L., Mendel J. T., Patton D. R., Ellison S. L., McConnachie A. W., 2011, *ApJS*, **196**, 11
Speagle J. S., Steinhardt C. L., Capak P. L., Silverman J. D., 2014, *ApJS*, **214**, 15
Teimoorinia H., Bluck A. F. L., Ellison S. L., 2016, *MNRAS*, **457**, 2086
Tomczak A. R., et al., 2016, *ApJ*, **817**, 118
Veilleux S., Osterbrock D. E., 1987, *ApJS*, **63**, 295
Whitaker K. E., et al., 2014, *ApJ*, **795**, 104
Whitaker K. E., et al., 2015, *ApJ*, **811**, L12
Wuyts S., et al., 2011, *ApJ*, **742**, 96

This paper has been typeset from a $\text{\TeX}/\text{\LaTeX}$ file prepared by the author.